Discover Nano

Discover

Research

A study of hydrogen plasma-induced charging effect in EUV lithography systems

Yao-Hung Huang[1] · Chrong Jung Lin[1] · Ya-Chin King[1]

Received: 22 November 2022 / Accepted: 9 February 2023

© The Author(s) 2023 OPEN

Abstract

In the extreme ultraviolet lithography system, EUV-induced hydrogen plasma charging effect is observed by in situ embedded micro-detector array. The 4k-pixel on-wafer array can detect and store the distributions of H_2 plasma in each in-pixel floating gate for non-destructive off-line read. The local uniformity of H_2 plasma intensity extracted by the threshold voltages on an array and its distributions across a wafer by the average bit cell current of MDAs provide insights into the detailed conditions inside advanced EUV lithography chambers.

Keywords Extreme ultraviolet (EUV) · Lithography · EUV-induced hydrogen plasma

Abbreviations

EUV Extreme ultraviolet
MDA Micro-detector array
BCC Bit cell current
ESP Energy sensing pad

Introduction

Extreme ultraviolet (EUV) lithography [1–3] is an optical patterning technology adopted in semiconductor processes for 7 nm technology node and beyond [4]. A CO_2 laser creates EUV radiation with a wavelength of 13.5 nm by shooting two consecutive laser pulses on a Sn droplet. The first low-intensity pulse flattens the Sn droplet into a pancake shape. The second high-intensity laser pulse vaporizes the Sn droplet to generate a plasma that emits EUV light [5]. During the de-excitation of the Sn plasma, some Sn atoms may accumulate on the incidence mirrors within the chamber, reducing their reflectivity. To maintain the mirrors' cleanliness, hydrogen gas is introduced to react with the Sn atoms, forming SnH_4 in a gaseous form, which can be easily removed through pumping [6, 7].

Hydrogen gas is transformed into high-density plasma under high-intensity EUV light, which ionizes the hydrogen gas, forming plasma that consists of ions, electrons, and neutral atoms. EUV light also excites the hydrogen atoms into higher energy levels. The interactions between the charges and neutral atoms determine the dynamics of the plasma, including

✉ Yao-Hung Huang, yhhuang.starlab@gapp.nthu.edu.tw | [1]Institute of Electronics Engineering, National Tsing Hua University, Hsinchu, Taiwan.

Springer

its temperature, density, and spectra [8–13]. In the commercial EUV lithography scanner [14–17], the EUV-induced hydrogen plasma needs to be investigated to understand its effect on the reliability and yield of the Si chips [18, 19].

EUV-induced hydrogen plasma can cause undesirable effects on the devices/circuits during lithography processes. Plasma-induced damage (PID) due to high-energy ions bombardment and charging damage induced by conduction current from plasma has been studied for structures that experience plasma-related treatments during manufacturing [20, 21]. PID can lead to degradations of device parameters such as threshold voltage, dielectric leakage current, and transconductance. As a result, detecting the plasma distribution and the charging effect during the process is essential. In this study, the EUV-induced hydrogen plasma charging effect is first-time reported and monitored by in situ embedded micro-detector array (MDA) [22]. The micro-detector's threshold voltage (V_{th}) and bit cell current (BCC) are used to analyze the magnitude and distribution of hydrogen plasma in the EUV lithography chambers.

Micro-detection array and operation principle

A FinFET-compatible MDA can monitor the EUV-induced plasma in the EUV lithography system. Figure 1 is the 3D structure of a 2 × 2 MDA, and a 4k-pixel array is fabrication on-wafer for follow-up experiments. First, each micro-detector comprises an Energy Sensing Pad (ESP) extended to the wafer surface and an n-channel floating-gate (FG) transistor for data storage and readout. ESPs are connected to the surface Al pads in the standard logic process, so they can collect charge induced by H_2 plasma in the EUV chamber. During the charging of ESPs during EUV processes, the potential of ESP is coupled to the FG by a laterally capacitively coupling structure between the contact slot and the FG. The coupled voltage from ESP will lead to changes in FG charge. To read out the stored FG charge, the source line (SL) and the bit line (BL) are connected to the source and drain terminal of the floating-gate-controlled n-channel FinFET, respectively. Through another coupling gate, read gate (RG), the channel current from SL to BL can then be measured through off-line wafer level tests.

Figure 2 is the Scanning Electron Microscope (SEM) cross-sectional view of a 4k MDA sample, where the ESPs are highlighted in yellow. The ESPs are directly connected to the top metal of the back end of line (BEOL) structure. In the SEM image, a Pt layer is coated on the samples to increase the SEM image's signal-to-noise ratio [23], which is not presented for regular detection in EUV chambers.

H_2 plasma charging effect in EUV chamber

Figure 3 illustrates the H_2 plasma-induced charging effect on the surface metal pad inside a EUV lithography chamber. When the EUV travels through projection optics and reticle, the low-pressure H_2 background gas in the chamber is excited into H_2 plasma [24, 25]. When the EUV is projected on ESPs, the electrons are ejected from the surface through the photoelectric effect, leading to a rise in the potential of ESP (V_{ESP}) rise when positive charges accumulate on the

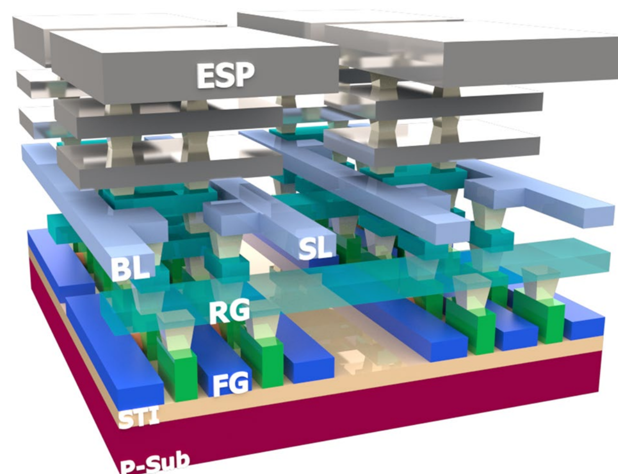

Fig. 1 3D structure of a 2 × 2 MDA

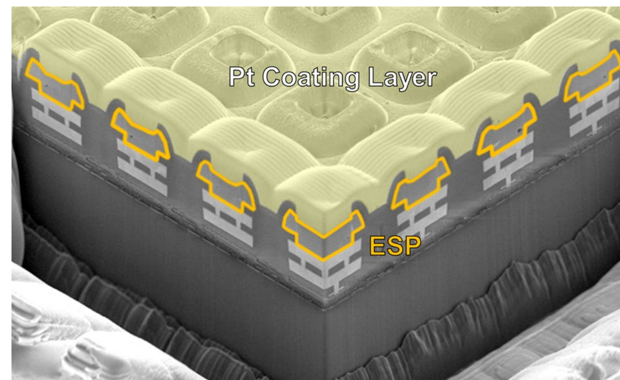

Fig. 2 SEM cross section of 4k-pixel MDA where ESPs are placed on the wafer surface. The MDA is coated with Pt to increase the SEM signal-to-noise ratio

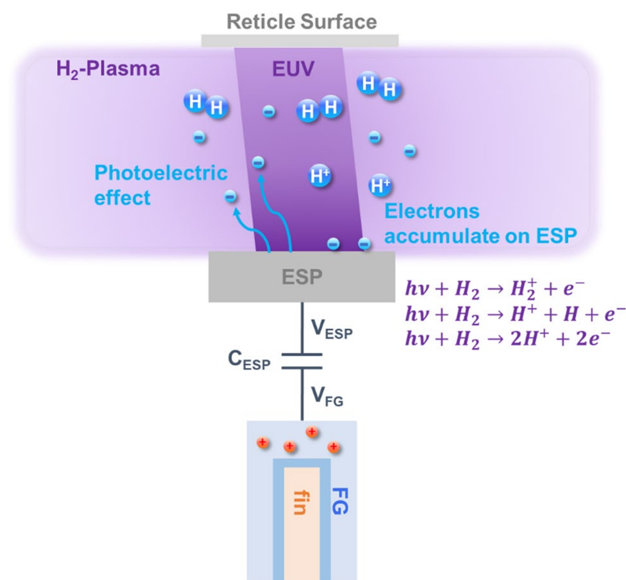

Fig. 3 Two different mechanisms—EUV photoelectric effect and H_2 plasma charging effects—are observed in the EUV system. Charge in FG can be altered as ESP is pulled to either high positive or negative potential charging

ESPs. Meanwhile, the negative charge generated by the H_2 plasma can be collected by the ESP, which causes V_{ESP} to drop accordingly. V_{ESP} is coupled to the potential of FG (V_{FG}) by the coupling structure, whose capacitance is C_{ESP}. After that, positive charges are drawn into FG through the gate dielectric by Fowler–Nordheim (FN) tunneling [26]. Therefore, the V_{th} of the micro-detector drops, whereas its bit cell current, i.e., BCC, increases under the same read condition. Since the amount of FG charge (Q_{FG}) is affected by both EUV exposure and plasma charging effect, EUV exposure experiments were carried out to characterize these two charging events, which co-occur on the ESP during EUV processes.

Experimental results and discussion

The on-wafer MDAs were sent into the EUV lithography system and were exposed to EUV of different dosages, from 0 to 20 mJ/cm^2. Figure 4 shows the bitmaps of threshold voltage (V_{th}) within the 4k-pixel array with a pixel pitch of 7.7 µm under different EUV exposure intensities. The V_{th} is extracted from the channel current of each pixel from the test detector array using the constant current method. Based on the experimental data, as EUV dosage increases, the measured V_{th}

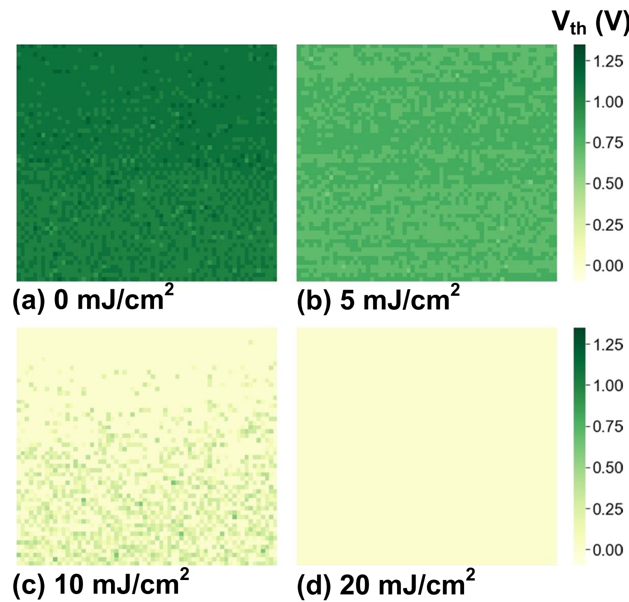

Fig. 4 Bitmap of V_{th} of the 4k MDA with array area of 500 μm × 500 μm before (**a**) and after exposure by increasing EUV dosage of **b** 5 mJ/cm^2, **c** 10 mJ/cm^2, **d** 20 mJ/cm^2, respectively

of floating-gate transistors drops as ESPs are charged by the electrons induced by H_2 plasma, leading to net positive FG charge change. The photoelectric effect increases the voltage of the ESP, leading to an increased attraction to negative charges. As a result, the net charge on ESP becomes negative. When the negative V_{ESP} is coupled to V_{FG}, the total charge in the FG increases, causing the V_{th} to decrease.

Before EUV exposure (0 mJ/cm^2), the bitmap shows a uniform level across the array area of 500 μm × 500 μm, without any failed bit. When the dosage increases to 10 mJ/cm^2, the V_{th} shift of the upper part is more significant than that of the lower part, which indicates that the local variation in charging of ESP may occur under high hydrogen plasma conditions. The regions with a higher V_{th} shift are more susceptible to PID. The estimated V_{ESP} level projected here can reach more than 8 V under this experiment condition.

Furthermore, the V_{th} distributions within the MDA can be analyzed by cumulative percentage, as shown in Fig. 5. Initially, the V_{th} of the MDA is about 1 V, see Fig. 4a, in a tight distribution. As expected, when negative charging of ESPs is dominated by plasma charging in EUV chambers, V_{th} shifts toward negative as the EUV dosage increases. Moreover, the local variations of hydrogen plasma lead to a wider V_{th} spread under high EUV dosage conditions. Finally, the V_{th} drops below zero as Q_{FG} becomes more positive, while the state of Q_{FG} can be reflected by the BCC levels.

Additionally, the exposure time is about 0.1 ms in the experiment, and V_{th} of all cells drop below zero under 20 mJ/cm^2. In typical scanners, exposure time per field is about 300 ms, and the MDA's response speed is high enough for *in*

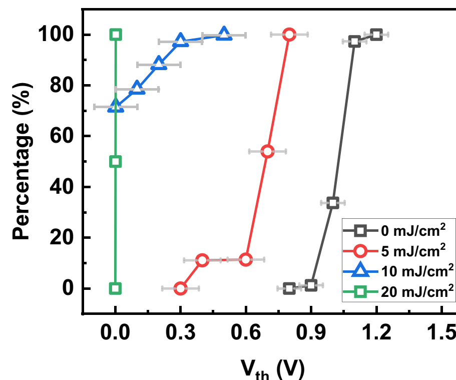

Fig. 5 V_{th} distributions within a 4k-pixel MDA. V_{th} drops as the plasma charges ESP after EUV exposure

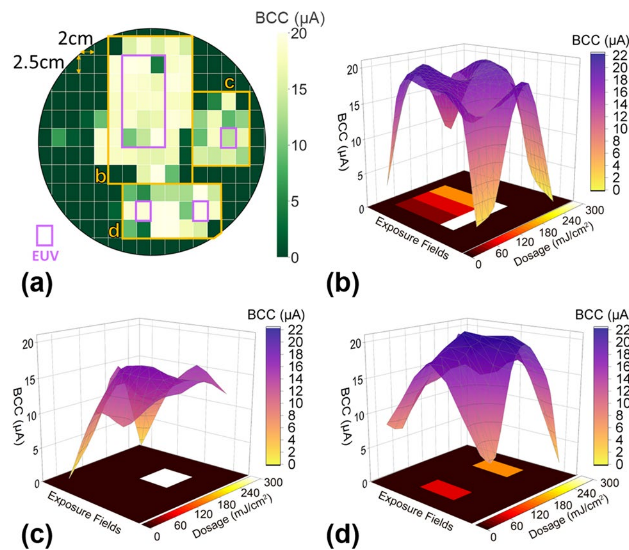

Fig. 6 **a** Wafer map of MDA bit cell current (BCC) after EUV exposure. **b**–**d** The bottom plots show the EUV dosage on multiple exposure fields, while the upper plots compare the average BCC from MDA on different parts of the wafer. The BCC saturates under high dosage exposure

situ H_2-induced plasma detection in lithography systems. Also, the current MDA can detect the hydrogen plasma charging effect resulting from a EUV exposure of 5 mJ/cm^2 differences, and its sensitivity can be controlled by the designing C_{ESP} of the MDA. When the C_{ESP} increases by using a longer contact slot, the sensitivity can be enhanced accordingly.

While the total response of MDAs combines the plasma charging effect and the photoelectric effect, the V_{th} can be mapped to a EUV exposure dosage. Therefore, the V_{th} shift can reflect the charging effect of H_2 plasma under different EUV dosages despite the presence of the photoelectric effect.

Figure 6a shows the average BCC of MDAs on a 12-inch wafer after the EUV exposure, where the dosage ranges from 30 to 300 mJ/cm^2. Four purple frames on the wafer indicate the reticles exposed to EUV. In Fig. 6b–d, the average BCC level over the whole MDA rises as the V_{th} becomes more negative. Moreover, the MDAs in adjacent exposed reticles are found to be subjected to the electron charging effect due to EUV-induced H_2 plasma. This suggested that the H_2 plasma-induced electrons spread wider than the exposed region, leading to more complex charging patterns on wafers, as shown in Fig. 6.

Conclusions

The EUV-induced H_2 plasma is analyzed by 4k-pixel on-wafer MDAs in the lithography chamber, and EUV parameters are extracted by the V_{th} and bit cell current from the MDA. The local distribution of plasma can be observed by a single MDA, while the distribution across the wafer can be monitored by MDAs placed in different reticle fields, and the spatial uniformity of plasma can be analyzed. The MDA can become a powerful tool, providing insight observations/on-wafer monitoring of the EUV-induced H_2 plasma inside future lithography chambers for future process optimization.

Acknowledgements The authors would like to thank the support from Taiwan Semiconductor Manufacturing Company (TSMC).

Author contributions All authors discussed and designed this research. YH carried out the experiments. YC and YH wrote the manuscript. All authors read and approved the final manuscript.

Funding This study is supported by Taiwan Semiconductor Manufacturing Company (TSMC).

Data availability The datasets generated during and/or analyzed during the current study are not publicly available due to the policy of our cooperative research company but are available from the corresponding author on reasonable request.

Declarations

Ethics approval and consent to participate Not applicable.

Consent for publication Not applicable.

Competing interests The authors declare that they have no competing interests.

Open Access This article is licensed under a Creative Commons Attribution 4.0 International License, which permits use, sharing, adaptation, distribution and reproduction in any medium or format, as long as you give appropriate credit to the original author(s) and the source, provide a link to the Creative Commons licence, and indicate if changes were made. The images or other third party material in this article are included in the article's Creative Commons licence, unless indicated otherwise in a credit line to the material. If material is not included in the article's Creative Commons licence and your intended use is not permitted by statutory regulation or exceeds the permitted use, you will need to obtain permission directly from the copyright holder. To view a copy of this licence, visit http://creativecommons.org/licenses/by/4.0/.

References

1. Fomenkov I, Brandt D, Ershov A, Schafgans A, Tao Y, Vaschenko G, Rokitski S, Kats M, Vargas M, Purvis M, Rafac R, La Fontaine B, De Dea S, LaForge A, Stewart J, Chang S, Graham M, Riggs D, Taylor T, Abraham M, Brown D. Light sources for high-volume manufacturing EUV lithography: Technology, performance, and power scaling. NANO. 2018. https://doi.org/10.1515/nano.0069.00001.
2. Levinson HJ. The potential of EUV lithography. In 35th European Mask and Lithography Conference (EMLC 2019); 2019. https://doi.org/10.1117/12.2528446
3. Benschop JP. EUV lithography: past, present and future. Extreme Ultraviolet (EUV) Lithography XII; 2021. https://doi.org/10.1117/12.2584527
4. Turkot B, Carson S, Lio A. Continuing Moore's law with EUV Lithography. In: 2017 IEEE International Electron Devices Meeting (IEDM); 2017. https://doi.org/10.1109/iedm.2017.8268390
5. Yang D-K, Wang D, Huang Q-S, Song Y, Wu J, Li W-X, Wang Z-S, Tang X-H, Xu H-X, Liu S, Gui C-Q. The development of laser-produced plasma EUV Light Source. Chip. 2022;1(3):100019. https://doi.org/10.1016/j.chip.2022.100019.
6. Braginsky OV, Kovalev AS, Lopaev DV, Malykhin EM, Rakhimova TV, Rakhimov AT, Vasilieva AN, Zyryanov SM, Koshelev KN, Krivtsun VM, van Kaampen M, Glushkov D. Removal of amorphous C and sn on mo:si multilayer mirror surface in hydrogen plasma and afterglow. J Appl Phys. 2012;111(9):093304. https://doi.org/10.1063/1.4709408.
7. van Herpen MMJW, Klunder DJW, Soer WA, Moors R, Banine V. Sn etching with hydrogen radicals to clean EUV optics. Chem Phys Lett. 2010;484(4–6):197–9. https://doi.org/10.1016/j.cplett.2009.11.030.
8. Bartnik A, Skrzeczanowski W, Wachulak P, Saber I, Fiedorowicz H, Fok T, Węgrzyński Ł. Low-temperature photoionized plasmas induced in XE gas using an EUV source driven by nanosecond laser pulses. Laser Part Beams. 2016;35(1):42–7. https://doi.org/10.1017/s0263034616000781.
9. Bartnik A, Wachulak P, Fiedorowicz H, Fok T, Jarocki R, Szczurek M. Extreme ultraviolet-induced photoionized plasmas. Physica Scr. 2014;1161:014061. https://doi.org/10.1088/0031-8949/2014/t161/014061.
10. Saber I, Bartnik A, Wachulak P, Skrzeczanowski W, Jarocki R, Fiedorowicz H. Temporal variations of electron density and temperature in KR/ne/h2photoionized plasma induced by nanosecond pulses from extreme ultraviolet source. Phys Plasmas. 2017;24(6):063501. https://doi.org/10.1063/1.4984254.
11. van der Horst RM, Beckers J, Osorio EA, Astakhov DI, Goedheer WJ, Lee CJ, Ivanov VV, Krivtsum VM, Koshelev KN, Lopaev DV, Bijkerk F, Banine VY. Exploring the electron density in plasma induced by EUV radiation: I. Experimental Study in hydrogen. J Phys D Appl Phys 2016;49(14):145203. https://doi.org/10.1088/0022-3727/49/14/145203
12. van der Horst RM, Osorio EA, Banine VY, Beckers J. The influence of the EUV spectrum on plasma induced by EUV radiation in argon and hydrogen gas. Plasma Sources Sci Technol. 2015;25(1):015012. https://doi.org/10.1088/0963-0252/25/1/015012.
13. Platier, B., van de Wetering, F. M., van Ninhuijs, M. A., Brussaard, G. J., Banine, V. Y., Luiten, O. J., Beckers, J. (2020). Addendum: Mapping electron dynamics in highly transient EUV photon-induced plasmas: a novel diagnostic approach using multi-mode microwave cavity resonance spectroscopy (2018 J. phys: D. Appl. phys. 52;034004). J Phys D Appl Phys 53(35), 359401. https://doi.org/10.1088/1361-6463/ab8f53
14. Pirati A, Peeters R, Smith D, Lok S, van Noordenburg M, van Es R, Verhoeven E, Meijer H, Minnaert A, van der Horst J-W, Meiling H, Mallmann J, Wagner C, Stoeldraijer J, Fisser G, Finders J, Zoldesi C, Stamm U, Boom H, Brandt D, Brown D, Fomenkov I, Purvis M. EUV lithography performance for manufacturing: Status and outlook. Extreme Ultraviolet (EUV) Lithography VII, 2016. https://doi.org/10.1117/12.2220423
15. Kim S-S, Chalykh R, Kim H, Lee S, Park C, Hwang M, Park J-O, Park J, Kim H, Jeon J, Kim I, Lee D, Na J, Kim J, Lee S, Kim H, Nam S-W. Progress in EUV lithography toward manufacturing. SPIE Proc. 2017. https://doi.org/10.1117/12.2264043.
16. van de Kerkhof M, Jasper H, Levasier L, Peeters R, van Es R, Bosker J-W, Zdravkov A, Lenderink E, Evangelista F, Broman P, Bilski B, Last T. Enabling sub-10nm node lithography: presenting the NXE:3400B EUV scanner. SPIE Proceedings doi. 2017;10(1117/12):2258025.
17. Smeets C, Salmaso G, Carbone J, Mastenbroek M, Benders N, van Es R, de Graaf R. 0.33 na EUV systems for high-volume manufacturing. Optical and EUV Nanolithography XXXV; 2022. https://doi.org/10.1117/12.2614220
18. van de Kerkhof M, Yakunin AM, Astakhov D, van Kampen M, van der Horst R, Banine V. EUV-induced hydrogen plasma: Pulsed mode operation and confinement in Scanner. J Micro Nanopattern Mater Metrol. 2021. https://doi.org/10.1117/1.jmm.20.3.033801
19. van de Kerkhof M, Yakunin AM, Kvon V, Nikipelov A, Astakhov D, Krainov P, Banine V. EUV-induced hydrogen plasma and particle release. Radiat Eff Defects Solids. 2022;177(5–6):486–512. https://doi.org/10.1080/10420150.2022.2048657.
20. Martin A. Review on the reliability characterization of plasma-induced damage. J Vac Sci Technol B Microelectron Nanometer Struct. 2009;27(1):426. https://doi.org/10.1116/1.3054356.

21. Eriguchi, K. (2017). Modeling of defect generation during plasma etching and its impact on electronic device performance—plasma-induced damage. Journal of Physics D: Applied Physics, 50(33), 333001. https://doi.org/10.1088/1361-6463/aa7523
22. Wang C-P, Lin BJ, Wu P-J, Shih J-R, Chih Y-D, Chang J, Lin CJ, King Y-C. Embedded micro-detectors for EUV exposure control in finfet CMOS technology. Nanoscale Res Lett. 2022. https://doi.org/10.1186/s11671-021-03645-5
23. Heu R, Shahbazmohamadi S, Yorston J, Capeder P. Target material selection for sputter coating of Sem Samples. Microscopy Today. 2019;27(4):32–6. https://doi.org/10.1017/s1551929519000610.
24. van de Ven TH, Reefman P, de Meijere CA, van der Horst RM, van Kampen M, Banine VY, Beckers J. Ion Energy distributions in highly transient EUV induced plasma in hydrogen. J Appl Phys. 2018;123(6):063301. https://doi.org/10.1063/1.5017303.
25. Beckers J, van de Ven T, van de Horst R, Astakhov D, Banine V. EUV-induced plasma: a peculiar phenomenon of a modern lithographic technology. Appl Sci. 2019;9(14):2827. https://doi.org/10.3390/app9142827.
26. Chiu F-C. A review on conduction mechanisms in dielectric films. Adv Mater Sci Eng. 2014;2014:1–18. https://doi.org/10.1155/2014/578168.

Publisher's Note Springer Nature remains neutral with regard to jurisdictional claims in published maps and institutional affiliations.